Intermetallics 19 (2011) 820–827

Contents lists available at ScienceDirect

Intermetallics

journal homepage: www.elsevier.com/locate/intermet

# Analysis of the plastic anisotropy and pre-yielding of ($\gamma/\alpha_2$)-phase titanium aluminide microstructures by crystal plasticity simulation

C. Zambaldi*, F. Roters, D. Raabe

*Max-Planck-Institut für Eisenforschung, Max-Planck-Strasse 1, Düsseldorf, Germany*

ARTICLE INFO

*Article history:*
Received 12 January 2011
Accepted 17 January 2011
Available online 11 March 2011

*Keywords:*
A. Titanium aluminides, based on TiAl
B. Brittleness and ductility
B. Mechanical properties at ambient temperature
B. Plastic deformation mechanisms
E. Mechanical properties, theory

ABSTRACT

The plastic deformation of lamellar microstructures composed of the two phases $\gamma$-TiAl and $\alpha_2$-$Ti_3Al$ is highly orientation dependent. In this paper we present a homogenized model that takes into account the micromechanical effect of the plate-like morphologies that are often observed in two-phase titanium aluminide alloys. The model is based on crystal elasto-viscoplasticity and 18 deformation systems were implemented that have been identified to govern the plastic flow of the lamellar microstructures. The model is validated against experiments on polysynthetically twinned (PST) crystals and shows good agreement with the data. On a larger length scale, the model is applied to a 64-grain aggregate to investigate the mechanical response of two different kinds of microstructures. Different magnitudes of the kinematic constraints exerted by the densely spaced and highly aligned interfaces are shown to affect the macroscopic flow behavior of the microstructures. The phenomenon of pronounced microplasticity of fully lamellar material as well as the stress variation inside two-phase microstructures are studied quantitatively.



## 1. Introduction

### 1.1. General introduction

$\gamma$-TiAl based microstructures with a minor volume fraction of the hexagonal $\alpha_2$-phase provide a good balance of properties for high temperature structural applications [1]. The significant intrinsic plastic anisotropy of the majority phase, near-stoichiometric $\gamma$-TiAl, as present in the two-phase ($\gamma/\alpha_2$)-microstructures, has recently been characterized by a combined experimental and computational study of the material flow during indentation [2]. This kind of microscale analysis is useful to identify the influence of alloy chemistry, such as aluminum content, ternary alloying elements, and impurities on the mechanical properties. However, for two-phase alloys it is known that the interfaces between the $\gamma$-variants and between $\gamma$-phase and $\alpha_2$-phase dominate the mechanics at the grain length scale. The kinematic constraints, resulting from the dense and aligned arrangement of the constituents, allow only a subset of their intrinsic plastic deformation mechanisms to operate.

In general, the effect of crystalline interfaces acting as strong barriers to dislocation motion is not included in the crystal plasticity finite element method (CPFEM). The explicit treatment of grain boundaries is difficult under a continuum mechanics based formulation such as the finite element method and possible implementations are investigated at the moment for disordered model materials [3,4]. At the same time, it is well known that $\gamma$-TiAl based alloys' desirable mechanical properties like toughness and creep resistance are closely related to the role of interfaces between the $\gamma$-phase and $\alpha_2$-phase and between the $\gamma$-domains [5].

To apply the crystal plasticity finite element method to the fine two-phase microstructures, a homogenized material model that incorporates the anisotropic flow behavior of two-phase microstructures on the length scale of lamellar grains was developed. Good agreement was found between experimental data and the simulated micromechanics in terms of the calculated yield stress anisotropy of polysynthetically twinned (PST) crystals with only one orientation of the lamellar planes. The pseudo single-phase model was extended to refined plate-like morphologies by varying the strength of kinematic constraints. Application of the model to simulations on a grain cluster gave insight into the field fluctuations and the pre-yielding of lamellar microstructures.

### 1.2. Flow anisotropy of polysynthetically twinned crystals

PST crystals can be grown by directional solidification of Al-lean TiAl and consist of one lamellar colony with only a single orientation of the lamellar planes [6]. Transmission electron microscopy (TEM) was widely used to characterize the fine-scaled lamellar microstructures with six orientation variants of the $\gamma$-phase [7,8].

* Corresponding author.
*E-mail address:* c.zambaldi@mpie.de (C. Zambaldi).

0966-9795/$ – see front matter © 2011 Elsevier Ltd. All rights reserved.
doi:10.1016/j.intermet.2011.01.012

Recently, an alternative method was presented to identify the order domains of the γ-phase by orientation microscopy in the scanning electron microscope (SEM) [9]. The SEM-based analysis allows for an improved quantification of the dimensions of the ordering domains because of the larger investigated areas compared to TEM characterization.

The anisotropic yielding behavior of two-phase lamellar titanium aluminide has been investigated experimentally on polysynthetically twinned (PST) crystals [7,8,10–15]. Some of the experimental data from the literature are given in Fig. 1. The strong flow stress anisotropy of PST crystals derives from the densely spaced interfaces in lamellar microstructures and is therefore closely related to Hall-Petch type effects in TiAl alloys [16,17]. The interfaces act as dislocation barriers and lead to an almost complete inhibition of deformation modes crossing the lamellar planes.

The types of operating deformation systems in γ-TiAl are known from TEM analysis. The plastic deformation of the $L1_0$-ordered γ-phase takes place by dislocation glide on {111}-planes [1]. Four ordinary dislocation systems with Burgers vector 1/2 $\langle 110\rangle$ and eight superlattice dislocation systems with Burgers vector $\langle 101\rangle$ have been reported frequently. Additionally, four {111} $\langle 11\overline{2}\rangle$ twinning systems were observed. In the $\alpha_2$-$Ti_3Al$ phase, dislocation glide with increasing critical shear strengths on prismatic, basal and pyramidal slip systems was found [18].

For the treatment of lamellar microstructures a different classification of deformation modes, based on the elongated morphology of the crystallites, was developed by Lebensohn et al. [19]. In that morphological classification three types of deformation modes were identified, namely the longitudinal, mixed and transversal type. This classification is important to interpret the different regimes of the uniaxial yield stress anisotropy of PST crystals and will be discussed in that respect in the following.

To investigate the uniaxial deformation of PST crystals it is useful to define a lamellar angle, $\Phi_L$, between the lamellar plane and the loading axis, Fig. 1(a). For a lamellar angle close to zero (lamellar interfaces parallel to the loading axis) the mixed mode deformation systems have the highest Schmid factors and are activated. The mixed mode deformation is taking place with Burgers vectors parallel to the lamellar interfaces and the slip planes are inclined to the interfaces at an angle of about 70°. Significant resistance against dislocation motion is expected since the dislocations interact with the interfaces and with dislocation half-loops protruding from the interfaces.

In the intermediate range of lamellar angles from 15° to 75°, the yield stresses are relatively low and this phenomenon is associated with dislocation glide on (111) planes parallel to the lamellar interfaces. This deformation mode is termed the longitudinal or easy glide mode in which the dislocations do not cross the lamellar boundaries.

For lamellar angles close to 90°, i.e. deformation perpendicular to the lamellar interfaces, the interfaces between $\alpha_2$-phase and γ-phase act as a strong dislocation barriers and the yield stress rises to its maximum value – the transversal mode of deformation governs the micromechanics. The transversal mode of deformation takes place with the slip planes and the Burgers vectors both being oriented at an angle with the interface plane.

Various approaches have been developed to model the anisotropic micromechanics of lamellar titanium aluminide microstructures. Apart from analytical models [16,13] also two- or three-dimensional crystal plasticity studies have been performed on the deformation of γ-TiAl based alloys since the pioneering work of Lee et al. [20]. Most of the later approaches root in the original crystal plasticity work of Peirce, Asaro and co-workers [21,22] who introduced the viscoplastic formulation of single crystal plasticity. The finite element method has been primarily applied for the solution of the field equations [23–28], but self-consistent schemes based on Eshelby's solution for a spherical inclusion have also been employed [19,29].

## 2. Selection of the effective slip systems for crystal plasticity finite element simulation

In previous works, crystal plasticity simulations have been applied to two-phase TiAl/$Ti_3Al$ microstructures in different ways. In the phase-resolved approaches the γ- and $\alpha_2$-phase were arranged according to their actual spatial distribution. Examples are the works of Fischer, Parteder, Schlögl, Marketz et al. [23,30], or of Werwer and Cornec [31,28]. In both cases the kinematic constraints were incorporated into either the mechanical model of the γ-phase or of both phases.

For these previous approaches, the computational effort arising from resolving the two phases makes the efficient study of the mechanical effect of different microstructures difficult. The material parameters applied to each phase, incorporate not only the intrinsic single-phase behavior but also the effect of the fine spatial distribution and the arrangement of the microstructural constituents. As discussed above, in the case of γ-TiAl based microstructures the constraint effect of the interfaces is often the governing factor on the micromechanics. The large strengthening effect from the interfaces needs to be distributed on the individual phases. Since the intrinsic single-phase properties as well as the effect of the interfaces are not easily quantified by experiments, the separate sets of parameters are difficult to validate and thus also difficult to interpret in a phase-resolved manner. At the same time a high level of discretization of space is necessary to apply the phase-resolved models which makes them computationally inefficient or even prohibitive for the study of realistic microstructures.

In the works of Kad et al. [32], Lebensohn [29], and later of Brockman [25] or of Grujicic and Batchu [24], a different modeling strategy was followed. Only the deformation modes relevant to the

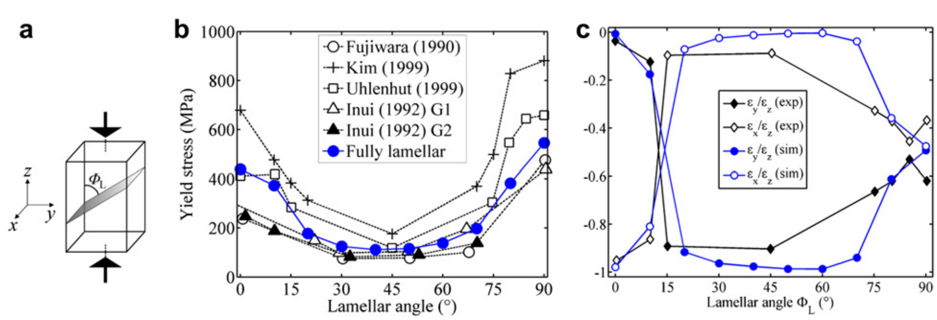


**Fig. 1.** Anisotropic yielding and anisotropic transverse deformation of PST crystals.(a) Definition of the lamellar angle, $\Phi_L$, with loading in tension or compression. (b) The simulated yield stresses show good agreement to the experimental data for the dependence on the inclination of the lamellar interfaces, $\Phi_L$. (c) The experimentally observed behavior of the relative transverse strains is captured by the model; experimental data from Uhlenhut [36]. In the coordinate system used, the lamellar plane rotates around the x-direction ([1 1 $\overline{2}$] of γ-M1) and uniaxial compression is applied along the z-direction.

kinematically constrained microstructures were incorporated into a single-phase crystal plasticity model. Since the need to resolve the spatial distribution of the different phases does not apply to this approach, grain aggregates can be modeled with moderate computational cost. Following these ideas, a similar approach was developed for a micromechanical description of two-phase $\gamma/\alpha_2$microstructures.

In theory, the full number of deformation systems for the $\alpha_2$-phase and the six orientational $\gamma$-variants, could be implemented into a CPFEM constitutive law. A total number of $6 \times 16 = 96$ systems for the six orientation variants of $\gamma$-TiAl, and additionally 12 systems from the hexagonal phase would have to be considered. The resulting 108 deformation systems would lead to a high computational effort for the CPFEM method. No implementation of such a model was attempted because the special crystallographic relations of the involved phases and deformation modes make possible a description with a smaller number of deformation systems. As it is assumed that the $\gamma$-phase order variants are present in comparable volume fractions in the lamellar microstructure, their cubic pseudo-symmetry can justify the contraction of their super- and ordinary dislocation systems to a single set of deformation modes which incorporate the effective behavior of both dislocation types. Following this approach also for the other deformation modes, the theoretical number of 108 deformation systems was systematically reduced to 18 systems of the following types:

- 3 effective systems for ordinary and superdislocation glide on the $(111)_\gamma$ lamellar plane;
- 3 effective (bi-directional) systems for twinning in the $(111)_\gamma$ lamellar plane; these are chosen bi-directional because the twinning shear in twin-related $\gamma$-variants has opposite signs in the coordinate system of the homogenized model;
- 6 effective systems to provide the transversal deformation mode; they were chosen identical to the pyramidal slip systems of the $\alpha_2$-phase and this decision is discussed in Section 5.1;
- 6 effective systems based on ordinary and superdislocation glide to implement the mixed mode deformation.

This simplified single-phase treatment assumes equal volume fractions of the $\gamma$-variants and a strict Blackburn orientation relationship, $(111)_\gamma \parallel (0001)_{\alpha_2}$ and $\langle 1\bar{1}0\rangle_\gamma \parallel \langle 11\bar{2}0\rangle_{\alpha_2}$, between the $\alpha_2$-phase and the $\gamma$-phase [33].

The resulting 18 deformation systems were implemented in an elasto-viscoplastic formulation of crystal plasticity. Different constitutive behaviors were prescribed for different modes of deformation. The deformation systems are listed in Table 1.

### 2.1. The crystal plasticity finite element method

The homogenized constitutive model was implemented as a subroutine in a commercial finite element code. For details of the employed elasto-viscoplastic model see for example Roters et al. [34] and Kalidindi et al. [35]. Only the equations that directly govern the shear rates of individual slip systems are given here: in crystal elasto-viscoplasticity the shear rates, $\dot{\gamma}^\alpha$, of the slip systems $\alpha$, are depending on the resolved shear stress, $\tau_c^\alpha$, by

$$\dot{\gamma}^\alpha = \dot{\gamma}_0 \left|\frac{\tau^\alpha}{\tau_c^\alpha}\right|^{1/m} \operatorname{sign}(\tau^\alpha) \qquad (1)$$

with material parameters $\dot{\gamma}_0$ and $m$. The critical resolved shear stress, $\tau_c^\alpha$, of individual slip systems $\alpha$ evolves with the shear rates, $\dot{\gamma}^\beta$, of all slip systems $\beta$, as $\dot{\tau}_c^\alpha = \sum_\beta h^{\alpha\beta}|\dot{\gamma}^\beta|$ with hardening matrix, $h^{\alpha\beta}$. The hardening matrix is calculated as $h^{\alpha\beta} = q^{\alpha\beta}h^{(\beta)}$, where the cross-hardening matrix, $q^{\alpha\beta}$, can hold different off-diagonal coefficients to include the effect of latent hardening, and the self-hardening contribution, $h^{(\beta)}$, is given by $h^{(\beta)} = h_0^\beta(1 - \tau^\beta/\tau_s^\beta)^{a^\beta}$. With these equations the parameters that govern the material flow are the initial critical shear strength, $\tau_0$, the saturation shear strength, $\tau_{s,}$ and $h_0$, which is influencing the initial self-hardening slope, and parameter, $a$, which governs the shape of the self-hardening curve but was kept constant at a value of 2.5 for all simulations. Also the reference shear rate, $\dot{\gamma}_0$, and the power-law exponent, $1/m$, were kept constant at $0.001\ \mathrm{s}^{-1}$ and 20, respectively.

**Table 1**
Slip systems of the homogenized material law; ‘M/T’ denotes systems that are present in the matrix family M = {M1,M2,M3} as well as the twin family T = {T1, T2, T3} of $\gamma$-TiAl-domains. Systems marked with ‘o/s’ will mainly deform by ordinary dislocations in specific domains but superdislocations could be activated in adjacent order domains to relief stress concentrations. Label ‘t’ denominates the effective twinning deformation modes in the $\gamma$-variants, implemented as three additional bi-directional shear systems, see text. The morphological classification following Lebensohn et al. [19] is also given.

| Number | Slip plane | Slip direction | Type | Morphology |
|---|---|---|---|---|
| 1 | $(111)^{M/T}$ | $[01\bar{1}]$ | o/s | Longitudinal |
| 2 | $(111)^{M/T}$ | $[10\bar{1}]$ | o/s | Longitudinal |
| 3 | $(111)^{M/T}$ | $[1\bar{1}0]$ | o/s | Longitudinal |
| 4 | $(111)^{M/T}$ | $[11\bar{2}]$ | t | Longitudinal |
| 5 | $(111)^{M/T}$ | $[1\bar{2}1]$ | t | Longitudinal |
| 6 | $(111)^{M/T}$ | $[\bar{2}11]$ | t | Longitudinal |
| 7 | $(11\bar{2}1)$ | $[\bar{1}\bar{1}2\ 6]$ | Pyramidal | Transversal |
| 8 | $(1\bar{2}11)$ | $[\bar{1}2\bar{1}6]$ | Pyramidal | Transversal |
| 9 | $(\bar{2}111)$ | $[2\bar{1}\bar{1}6]$ | Pyramidal | Transversal |
| 10 | $(\bar{1}\bar{1}21)$ | $[11\bar{2}6]$ | Pyramidal | Transversal |
| 11 | $(\bar{1}2\bar{1}1)$ | $[1\bar{2}16]$ | Pyramidal | Transversal |
| 12 | $(2\bar{1}\bar{1}1)$ | $[\bar{2}11\ 6]$ | Pyramidal | Transversal |
| 13 | $(\bar{1}11)^M$ | $[0\bar{1}1]$ | o/s | Mixed |
| 14 | $(1\bar{1}1)^M$ | $[10\bar{1}]$ | o/s | Mixed |
| 15 | $(11\bar{1})^M$ | $[1\bar{1}0]$ | o/s | Mixed |
| 16 | $(\bar{1}11)^T$ | $[\bar{1}01]$ | o/s | Mixed |
| 17 | $(11\bar{1})^T$ | $[01\bar{1}]$ | o/s | Mixed |
| 18 | $(11\bar{1})^T$ | $[\bar{1}10]$ | o/s | Mixed |

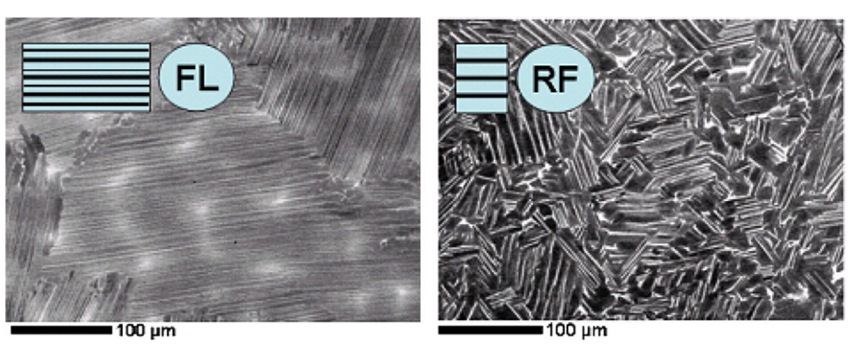


**Fig. 2.** Fully lamellar (FL, left) and refined (RF, right) microstructures of Ti–46Al–8Nb; BSE imaging mode, the refined microstructure is taken from Wu and Hu ([38], Fig. 1).

**Table 2**
Parameters of the homogenized crystal plasticity model, m = 0.05, $\dot{\gamma}_0 = 0.001\ s^{-1}$. The numbering of the effective slip systems is according to Table 1. Two sets of parameters were defined for the fully lamellar (FL) and the refined (RF) or convoluted microstructure.

| No. | Type | $\tau_0$, MPa | $\tau_s$, MPa | $h_0$, MPa | a |
|---|---|---|---|---|---|
| 1–6 | FL, easy glide | 50 | 500 | 1000 | 2.5 |
| 1–6 | RF, easy glide | 117 | 1167 | 1000 | 2.5 |
| 7–18 | FL, mixed and transversal | 250 | 2500 | 1000 | 2.5 |
| 7–18 | RF, mixed and transversal | 225 | 2250 | 1000 | 2.5 |

## 3. Application of the homogenized material law to the anisotropic plasticity of PST crystals

Numerical experiments were carried out with different sets of parameters and the model matched the findings from experiments on PST crystals well. The well-known anisotropic yielding behavior, Section 1.2, was accurately predicted, Fig. 1(b). The experiments as well as the simulations, show a pronounced yield stress minimum for inclinations of the lamellar interface of approximately 20°–70° from the loading axis.

Furthermore, the orientation dependent relative transverse strains, Fig. 1(c), also showed good agreement with experiments for the same set of parameters. When the lamellar plane is parallel to the loading axis ($\Phi_L \approx 0°$) the change in length perpendicular to the lamellar interfaces is negligible. All lateral strain is accommodated in the direction along the lamellar interface and perpendicular to the loading axis. If the loading direction is normal to the lamellar plane ($\Phi_L \approx 90°$), the lateral strains are equal and amount to about minus one half of the strain in loading direction. In-depth analyses of this channeling of deformation are given in the literature [8,14,36].

The simulated results in Fig. 1 are in agreement with the data of Uhlenhut [37]. By changing the constitutive parameters of the model the other experimental results obtained for PST crystals of different microstructures under uniaxial tension and compression could also be matched by the model.

## 4. Application of the homogenized law to two different microstructures

### *4.1. Extension of the model to microstructures refined by solid state phase transformation*

The presented constitutive model accurately describes the plastic deformation of the two-phase lamellar microstructures. In conjunction with the flexibility of the finite element method to solve complex boundary value problems, the simulation of realistic microstructures was possible. To investigate the effect of the arrangement of the constituent phases on the mesoscopic (grain length scale) and macroscopic (sample length scale) deformation characteristics, two types of microstructures were targeted for the simulations: the first type was the fully lamellar (FL) microstructure, Fig. 2(a). Neglecting the hardening from the boundaries of the lamellar colonies, it was simulated with the previously identified parameters for the PST crystals.

For the second type of material, the `convoluted' microstructure was chosen, Fig. 2(b). It is an example for the general case of a refined (RF) microstructure; it results from a quenching and annealing heat treatment which has previously been investigated as a way to refine Ti-Al microstructures through solid state phase transformation [38]. Cast material with a convoluted microstructure was reported to exhibit a improved room temperature ductility when compared to the fully lamellar microstructures [39]. With a Hall-Petch type argument, the crystal plasticity model was extended to the refined (RF) microstructure. It is not possible to study the small lamellar-like bundles of the convoluted structure for their micromechanics experimentally, as in the case of PST crystals. For the simulations, they were expected to show less plastic anisotropy because of shorter and wider 'lamellar-like' plates.

In the employed Hall-Petch type approach, shortening of a microstructural dimension resulted in a higher shear resistance of the deformation systems along the corresponding direction and

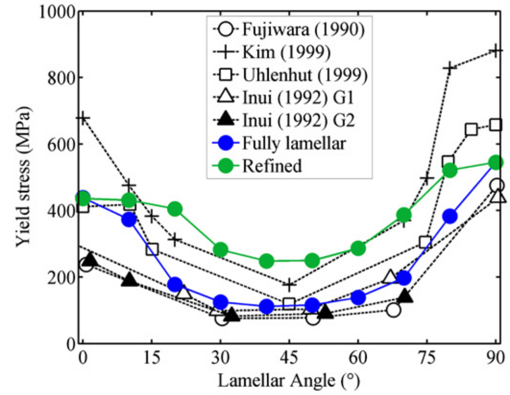


**Fig. 4.** Yield stress dependence on the lamellar angle, for the lamellar (FL) microstructure and for the refined (RF) microstructure.

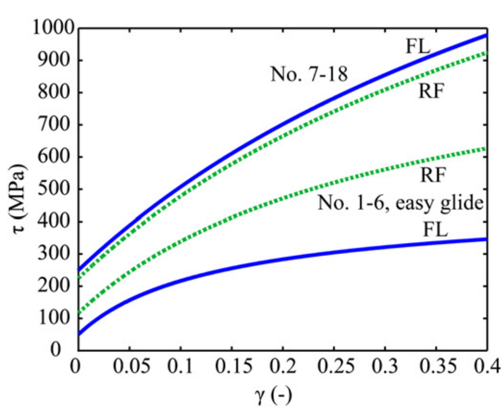


**Fig. 3.** The chosen self-hardening behaviors (Table 2) of the deformation systems inside the lamellar (FL) and the convoluted (RF) microstructure; shear strength, $\tau$, versus plastic shear, $\gamma$. The numbering of deformation systems refers to Table 1.

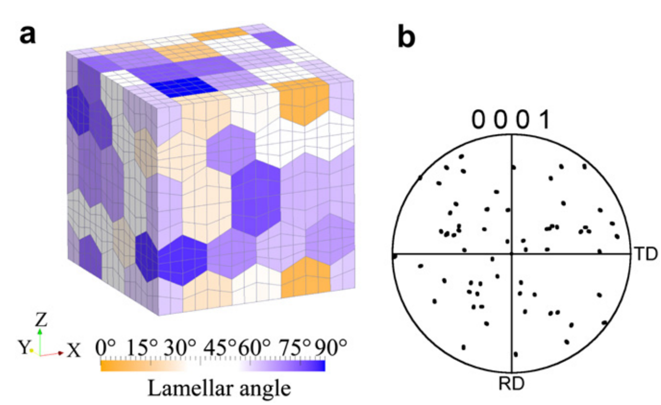


**Fig. 5.** (a) Finite element mesh of the periodic 64-grain model; the lamellar angle, $\Phi_L$, between the lamellar interfaces and the tensile axis, Z, is indicated. Soft grains are white, hard grains with angles of the lamellar planes near 0° and near 90° are shown in two different colors. (b) (0001) pole figure of the 64 random grain aggregate.

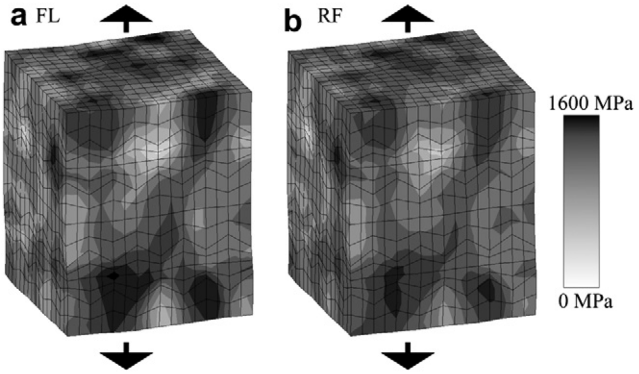


**Fig. 6.** Simulated distribution of the axial stress component in the 64-grain model at 10% elongation. The simulation result based on parameters for the FL microstructure shows higher stress contrast throughout the microstructure.

lengthening in lower shear resistance. The approach follows the picture of a reduction or extension of the mean free path that dislocations can glide before reaching an obstacle. Especially the minimum yield stresses that originate from easy glide along the lamellar planes were expected to be significantly stronger in the refined microstructure because of the fragmented arrangement of the stacked plates of $\gamma$-phase and $\alpha_2$-phase. The chosen hardening parameters are given in Table 2 for both types of microstructures. In order to keep the number of constitutive parameters as small as possible, deformation systems 1–6 from Table 1 were treated identically. Also the mixed and transversal modes of deformation were assigned only one common set of crystal plasticity parameters.

The corresponding self-hardening is shown in Fig. 3 and the resulting two kinds of simulated yield stress anisotropy are given in Fig. 4. While the lamellar interface in the FL microstructure is identical to a {111}-plane which is also parallel to the {0001}-basal plane of the $\alpha_2$-phase, in the convoluted (RF) microstructure, the definition of a lamellar interface is not as clear. Nevertheless, the $\alpha_2$-phase precipitates on the {111}-planes of the massively transformed $\gamma$-phase and therefore the crystallographic relations are expected to be similar to the lamellar case. Consequently, in the following, the poly-twinned order domain structure found in lamellar material will also be assumed for the refined microstructure.

### 4.2. Simulation of polycrystal material

With the developed homogenized model a cluster of 64 periodically arranged grains was simulated under tensile deformation, Fig. 5. The shape of the identical grains was derived from a rhombohexagonal dodecahedron. The grains were assigned random orientations. Periodic displacement boundary conditions were applied to the aggregate in order to minimize surface effects. The constitutive parameters were chosen either to represent the fully lamellar (FL) microstructure or the refined (RF or 'convoluted') microstructure. The crystal plasticity formulation does not contain a physical length scale. Therefore, for both microstructures the same finite element model was used. It follows that the corresponding physical volume of material was much smaller for the model with convoluted microstructure in comparison to the fully lamellar model.

Fig. 6 shows the distribution of the axial tensile stresses throughout the microstructure, for both sets of parameters. Strong fluctuations between differently oriented grains are present. Stress levels of few hundred MPa can be observed in some locations, whereas other regions are showing stresses that are significantly larger than 1000 MPa. While the stress distribution is qualitatively identical for both sets of crystal plasticity parameters, the FL microstructure, Fig. 6(a), shows higher stress contrast. However, the analysis up to now was limited to the surface of the model.

In order to take into account the full 3-dimensional results of the simulations, the averaged axial stress per grain plotted against the average axial strain is given in Fig. 7 for the two cases. For the material law representing the convoluted (RF) microstructure, again a narrower stress distribution was observed. Especially the maximum stress levels at the initial stages of plasticity are reduced by about 100 MPa.

## 5. Discussion

### 5.1. Model formulation

The homogenized model takes into account only the deformation systems of ($\gamma/\alpha_2$) two-phase titanium aluminide microstructures that have been reported to be highly active during plastic deformation. For incorporation into the crystal plasticity model, the decision had to be made whether to include the transversal slip systems only from the $\gamma$-phase, only from the $\alpha_2$-phase, or from both phases. The relative barrier strengths of the boundaries are not known and the mechanical properties of the very thin $\alpha_2$-lamellae can only be guessed. Because quantitative information on the relative strength contributions is not available, and to increase computational efficiency, only the six pyramidal slip systems from the $\alpha_2$-phase were taken into account. They are well-suited to represent the translamellar, i.e. the transversal, deformation mode. The transversal slip systems of the $\gamma$-phase twin and matrix

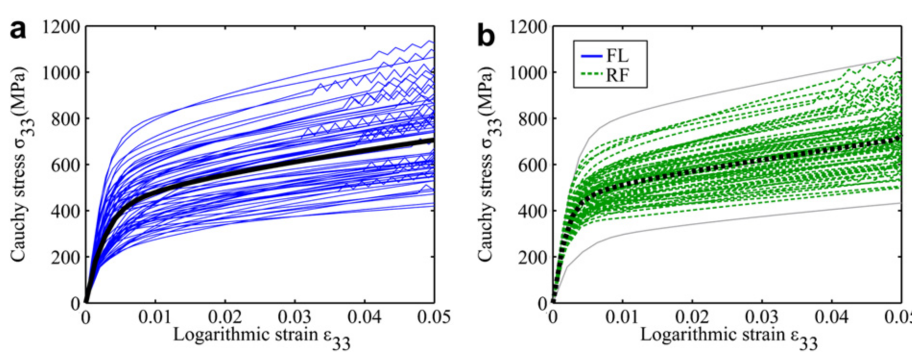


**Fig. 7.** The individual flow curves from the 64 grains (averaged over the 64 elements per grain) are shown for the parameter sets reflecting the (a) fully lamellar (FL) microstructure and (b) the refined (RF) microstructure; in (b) also the two curves on the highest and lowest stress level from the FL microstructure are shown for better comparison. Higher maximum and lower minimum values are apparent for the FL simulation. Average stress–strain curves for the two materials are drawn in bold. The same set of 64 random grain orientations was used in both simulations. Zig-zag shaped stress fluctuations in some of the curves are assumed to originate from instabilities during the evaluation of the periodic boundary conditions.

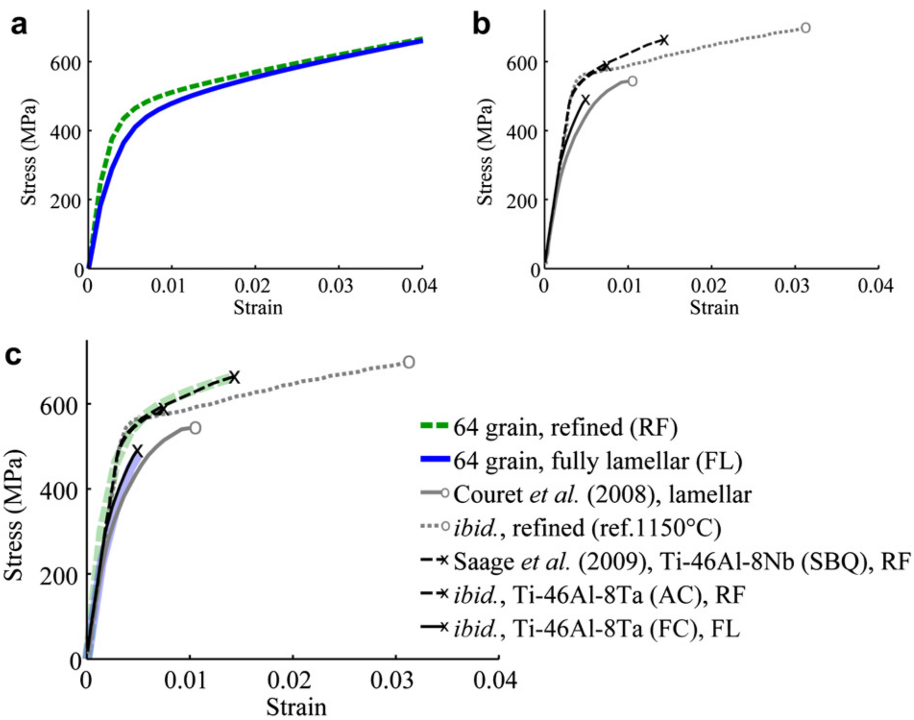


**Fig. 8.** Flow curves of simulated 64-grain clusters with FL (−) and refined (− −) microstructures, (a), compared to literature data measured at room temperature [46,39], (b). The bold, semi-transparent curves in (c) are the scaled results from the respective simulations and match the experimental curves from Saage et al. [39] almost perfectly; in Saage et al. [39] the furnace cooled (FC) microstructure was lamellar, whereas the air cooled (AC) and salt bath quenched (SBQ) microstructures exhibited a refined ('convoluted') microstructure. The material with ductility over 1% contained 8-at.% tantalum.

variants would have made necessary the consideration of at least 12 ordinary and super dislocation systems and 6 twin systems and would have resulted in longer computation times with negligible additional value for the simulation capabilities.

### 5.2. Validation, extension and application of the model

The model was validated against experimental data on the deformation of PST crystals and showed good agreement for the yield stress anisotropy and the relative transversal stresses as reported by Uhlenhut [37]. The model was then extended to the refined microstructures that could also be described as a highly disturbed case of a lamellar microstructure. This extension to another type of microstructure enabled a comparative study of predicted flow curves from a multi-grain finite element model. Porter et al. [40] have recently demonstrated that the anisotropic plasticity of PST microstructures is also found in lamellar micropillars of just a few ten micrometers in diameter and those findings support the assumption that fully lamellar microstructures could be treated equivalent to a space filling aggregate of PST crystals.

The simulation results could help to explain the improved ductility of the convoluted microstructure that was observed in experiments [39]. The present model does not make any predictions on the nucleation of cracks.[1] However, under the influence of the high peak stresses in the lamellar microstructure, a once formed microcrack is assumed to reach a critical size much faster than in the refined microstructure. It is noteworthy that the reduction in peak stresses was mainly achieved by strengthening the 'easy glide' deformation along the plates in the convoluted (RF) structure in comparison to the lamellar structure.

### 5.3. Interpretation of the pre-yielding phenomenon in fully lamellar microstructures and the mechanical effect of microstructural refinement

The findings on stress and strain fluctuations inside the microstructure cannot be easily confirmed experimentally.[2] However, another result was found from the simulated flow curves which could be directly compared to the existing experimental data: the previously investigated pre-yielding behavior of fully lamellar microstructures [44,45,39]. Fig. 8 compares the simulated stress–strain curves to experimental flow curves of fully lamellar material and two types of refined microstructures. Generally, the refined microstructures exhibit a defined transition from elastic to plastic deformation, whereas the lamellar microstructures show significant microplasticity at relatively low stresses.

The pre-yielding in lamellar microstructures is not discussed explicitly in the work of Couret et al. [46] on extruded TiAl alloys. The shown flow curves, however, exhibit pronounced pre-yielding in the lamellar microstructures. Also given are the flow curves of a duplex microstructure that shows no pre-yielding but a well-defined yield point. Pre-yielding is assumed to be identical to what Dimiduk et al. [16] termed a *gradual yield transient* for their results from compression testing on fully lamellar polycrystals. Also Kim [47] discussed the *low microyielding stresses* of lamellar microstructures in contrast to the defined yield point of duplex material and found the pre-yielding to be less pronounced for small lamellar grain sizes in the observed range from 2500 μm to 230 μm.

The deviation from linearity in the simulated flow curves is to some extent an inherent feature of the underlying elasto-

[1] See Bieler et al. [41] for an in-depth study of crack nucleation in γ-TiAl microstructures.

[2] For an optical strain mapping approach to Ti–Al microplasticity see Chang et al. [42] and Jiang et al. [43].

viscoplastic formulation of the material law. Nevertheless, the simulation of the refined microstructure clearly showed a sharper yielding behavior than the fully lamellar model. Through a linear scaling of the simulated flow curves by a factor of about 1.2, an almost perfect match to the experimental data from tensile testing on Ti–46Al–8(Nb/Ta) alloys [39] could be achieved. The justification for the scaling operation is the different composition of the material used in the experiments. The crystal plasticity parameters were identified based on data of binary PST crystals. Addition of large atoms such as Nb or Ta leads to a reduction of the lamellar spacing and also refines the dimensions of the convoluted microstructure. For the alloyed material an increased stress level is expected because of this structural refinement [48].

The simulation results suggest that the strength of the easy glide mode dominates the micromechanical behavior in γ-TiAl based two-phase alloys. If the easy glide mode is strengthened by a refinement of the microstructure, the plastic anisotropy inside the microstructure is reduced. As a consequence, a significant increase in the stresses required to initiate plastic flow and a reduction of the stress concentration in hard-oriented grains can be achieved at the same time. Thereby, the issues of pre-yielding as well as the low ductility of the two-phase alloys could be overcome.

## 6. Conclusions

A crystal plasticity model was presented which describes the micromechanical response of kinematically constrained γ-TiAl based microstructures by incorporating the relevant deformation modes. It was demonstrated that the model quantitatively captures the plastic anisotropy of $(\gamma/\alpha_2)$-two-phase microstructures. The model was validated against experimental data on PST crystals. It showed good agreement with the orientation dependent uniaxial yield stress as well as the relative transversal strains.

Through simulation of polycrystalline aggregates it was shown that the pre-yielding phenomenon in fully lamellar alloys is presumably related to the plastic anisotropy of the lamellar colonies. The weakest grains with lamellar angles against the loading axis of around 45° start to yield at low stresses during uniaxial loading of a lamellar microstructure. The early yielding of grains with soft orientations at the same time leads to higher stresses in the hard-oriented grains. This stress contrast between hard and soft grains could be an important reason for the very low ductility of polycrystalline lamellar material at low and intermediate temperatures.

On the methodological side of CPFEM constitutive modeling it could be concluded that periodic boundary conditions enable a realistic correlation between CPFEM simulation results and experimental data, even at relatively low resolutions of the microstructure. The minimum number of 200 grains in a sample cross section that was requested for experimental studies by Kad and Asaro [49] can be reduced in CPFEM modeling through the use of periodic boundary conditions.

The excellent agreement between the simulations and experiments for the incipient plastic deformation, demonstrates the potential of the applied CPFEM technique to quantitatively describe the micromechanics of γ-TiAl based alloys. It further indicates that the most relevant micromechanical features of the microstructures were accounted for by the model.

## Acknowledgements

We acknowledge valuable remarks by R. Lebensohn (Los Alamos National Laboratory). This work was performed within the EU FP6 integrated project IMPRESS (NMP3-CT-2004-500635).

## References

[1] Appel F, Wagner R. Microstructure and deformation of two-phase gamma-titanium aluminides. Materials Science and Engineering 1998;R22:187–268. doi:10.1016/S0927-796X(97)00018-1.
[2] Zambaldi C, Raabe D. Plastic anisotropy of γ-TiAl revealed by axisymmetric indentation. Acta Materialia 2010;58(9):3516–30. doi:10.1016/j.actamat.2010.02.025.
[3] Ma A, Roters F, Raabe D. On the consideration of interactions between dislocations and grain boundaries in crystal plasticity finite element modeling – theory, experiments, and simulations. Acta Materialia 2006;54(8):2181–94. doi:10.1016/j.actamat.2006.01.004.
[4] Ma A, Roters F, Raabe D. Studying the effect of grain boundaries in dislocation density based crystalplasticity finite element simulations. International Journal of Solids and Structures 2006;43(24):7287–303. doi:10.1016/j.ijsolstr.2006.07.006.
[5] Dimiduk DM, Parthasarathy TA, Hazzledine PM. Design-tool representations of strain compatibility and stress–strain relationships for lamellar gamma titanium aluminides. Intermetallics 2001;9(10–11):875. doi:10.1016/S0966-9795(01)00085-1.
[6] Takeyama M, Yamamoto Y, Morishima H, Koike K, Chang SY, Matsuo T. Lamellar orientation control of Ti–48Al PST crystal by unidirectional solidification. Materials Science and Engineering A 2002;329 and 331:7–12. doi:10.1016/S0921-5093(01)01493-9.
[7] Inui H, Oh M, Nakamura A. Room-temperature tensile deformation of polysynthetically twinned (PST) crystals of TiAl. Acta Metallurgica et Materialia 1992;40(11):3095–104.
[8] Kishida K, Inui H, Yamaguchi M. Deformation of lamellar structure in TiAl–Ti3Al two phase alloys. Philosophical Magazine A 1998;78:1–28.
[9] Zambaldi C, Zaefferer S, Wright S. Characterization of order domains in gamma-TiAl by orientation microscopy based on electron backscatter diffraction. Journal of Applied Crystallography 2009;42(6):1092–101. doi:10.1107/S0021889809036498.
[10] Fujiwara T, Nakamura A, Hosomi M, Nishitani SR, Shirai Y, Yamaguchi M. Deformation of polysynthetically twinned crystals of TiAl with a nearly stoichiometric composition. Philosophical Magazine A 1990;61(4):591–606.
[11] Yamaguchi M. Deformation and recrystallization behaviour of the TiAl phase constituting the TiAl/Ti3Al lamellar structure of Ti-rich TiAl compounds. ISIJ International 1991;31(10):1127–33. doi:10.2355/isijinternational.31.1127.
[12] Umakoshi Y, Nakano T, Yamane T. The effect of orientation and lamellar structure on the plastic behavior of TiAl crystals. Materials Science and Engineering A 1992;152(1–2):81–8.
[13] Hazzledine P, Kad B. Yield and fracture of lamellar γ/α2 Tial alloys. Materials Science and Engineering A 1995;192/193:340–6.
[14] Kim M, Nomura M, Vitek V, Pope D. Deformation of PST Tial single crystals with near-hard orientations. In: George E, Yamaguchi M, Mills M, editors. Materials Research Society Symposium Proceedings, 552; 1999. p. KK3.1.1.
[15] Lapin J, Gabalcová Z, Bajana O. The effect of microstructure on mechanical properties of directionally solidified intermetallic Ti–46Al–8Nb alloy. Kovove Materiály 2009;47:159–67.
[16] Dimiduk DM, Hazzledine P, Parthasarathy T, Seshagiri S, Mendiratta M. The role of grain size and selected microstructural parameters in strengthening fully lamellar TiAl alloys. Metallurgical and Materials Transactions A 1998;29(1):37–47.
[17] Maruyama K, Yamaguchi M, Suzuki G, Zhu H, Kim HY, Yoo M. Effects of lamellar boundary structural change on lamellar size hardening in TiAl alloy. Acta Materialia 2004;52:5185–94.
[18] Kishida K, Takahama Y, Inui H. Deformation twinning in single crystals of a D019 compound with an off-stochiometric composition (Ti–36.5 at.%Al). Acta Materialia 2004;52:4941–52.
[19] Lebensohn R, Uhlenhut H, Hartig C, Mecking H. Plastic flow of gamma-Tial-based polysynthetically twinned crystals: micromechanical modeling and experimental validation. Acta Materialia 1998;46(13):4701–9.
[20] Lee BJ, Ahzi S, Kad BK, Asaro RJ. On the deformation mechanisms in lamellar Ti–Al alloys. Scripta Metallurgica et Materialia 1993;29(6):823–8.
[21] Peirce D, Asaro RJ, Needleman A. Material rate dependence and localized deformation in crystalline solids. Acta Metallurgica 1983;31(12):1951–76. doi:10.1016/0001-6160(83)90014-7.
[22] Asaro RJ, Needleman A. Overview 42. Texture development and strain-hardening in rate dependent polycrystals. Acta Metallurgica 1985;33(6):923–53.
[23] Schlögl SM, Fischer FD. The role of slip and twinning in the deformation behaviour of polysynthetically twinned crystals of Tial: a micromechanical model. Philosophical Magazine A 1997;75(3):621–36. doi:10.1080/01418619708207193.
[24] Grujicic M, Batchu S. A crystal plasticity materials constitutive model for polysynthetically-twinned gamma-Tial+alpha(2)–Ti3Al single crystals. Journal of Materials Science 2001;36(12):2851–63.
[25] Brockman RA. Analysis of elastic-plastic deformation in TiAl polycrystals. International Journal of Plasticity 2003;19(10):1749. doi:10.1016/S0749-6419(02)00102-X.
[26] Marketz W, Fischer F, Clemens H. Deformation mechanisms in TiAl intermetallics—experiments and modeling. International Journal of Plasticity 2003;19:281–321.
[27] Roos A, Chaboche JL, Gelebart L, Crepin J. Multiscale modelling of titanium aluminides. International Journal of Plasticity 2004;20(4):811–30.
[28] Werwer M, Cornec A. The role of superdislocations for modeling plastic deformation of lamellar TiAl. International Journal of Plasticity 2006;22(9):1683–98. doi:10.1016/j.ijplas.2006.02.005.

[29] Lebensohn R. Modelling the role of local correlations in polycrystal plasticity using viscoplastic selfconsistent schemes. Modelling and Simulation in Materials Science and Engineering 1999;7(5):739–46.
[30] Schlögl S, Fischer F. Numerical simulation of yield loci for PST crystals of Tial. Materials Science and Engineering A 1997;239–240:790–803. doi:10.1016/S0921-5093(97)00668-0.
[31] Werwer M, Cornec A. Numerical simulation of plastic deformation and fracture in polysynthetically twinned (PST) crystals of TiAl. Computational Materials Science 2000;19(1):97–107.
[32] Kad BK, Dao M, Asaro RJ. Numerical simulations of plastic-deformation and fracture effects in 2 phase gamma-Tial+alpha-2-Ti3Al lamellar microstructures. Philosophical Magazine A 1995;71(3):567–604.
[33] Blackburn M. Some aspects of phase transformations in titanium alloys. In: Jaffee R, Promisel N, editors. The science, technology and applications of titanium; proceedings of a conference held 1968 in London. Pergamon Press; 1970. p. 633.
[34] Roters F, Eisenlohr P, Hantcherli L, Tjahjanto DD, Bieler TR, Raabe D. Overview of constitutive laws, kinematics, homogenization, and multiscale methods in crystal plasticity finite element modeling: theory, experiments, applications. Acta Materialia 2010;58(4):1152–211. doi:10.1016/j.actamat.2009.10.058.
[35] Kalidindi SR, Bronkhorst CA, Anand L. Crystallographic texture evolution in bulk deformation processing of fcc metals. Journal of the Mechanics and Physics of Solids 1992;40(3):537–69. doi:10.1016/0022-5096(92)80003-9.
[36] Paidar V, Yamaguchi M. Constrained deformation of a lamellar structure. Materials Science and Engineering: A 2007;462(1–2):460–4. doi:10.1016/j.msea.2006.01.180.
[37] Uhlenhut H. Ursachen plastischer Anisotropie von $\gamma$-TiAl Basislegierungen. Shaker Verlag; 1999.
[38] Wu X, Hu D. Microstructural refinement in cast Tial alloys by solid state transformations. Scripta Materialia 2005;52(8):731–4. doi:10.1016/j.scriptamat.2004.12.021.
[39] Saage H, Huang A, Hu D, Loretto M, Wu X. Microstructure and tensile properties of massively transformed and aged Ti46Al8Nb and Ti46Al8Ta alloys. Intermetallics 2009;17:32–8.
[40] Porter W, Uchic M, John R, Barnas N. Compression property determination of a gamma titanium aluminide alloy using micro-specimens. Scripta Materialia 2009;61(7):678–81. doi:10.1016/j.scriptamat.2009.05.038.
[41] Bieler T, Eisenlohr P, Roters F, Kumar D, Mason D, Crimp M, et al. The role of heterogeneous deformation on damage nucleation at grain boundaries in single phase metals. International Journal of Plasticity 2009;25:1655–83. doi:10.1016/j.ijplas.2008.09.002.
[42] Chang S, Chiang FP, Rosenberger A. A micromechanics study of lamellar Tial. Experimental Mechanics 2006;46:173–8.
[43] Jiang H, Garcia-Pastor F, Hu D, Wu X, Loretto M, Preuss M, et al. Characterization of microplasticity in Tial-based alloys. Acta Materialia 2009;57(5):1357–66. doi:10.1016/j.actamat.2008.11.029.
[44] Wu X, Hu D, Loretto M. The influence of microstructure and surface residual stresses on pre-yield cracking in Tial alloys. Gamma Titanium Aluminides; 2003:517–20.
[45] Hu D, Huang A, Jiang H, Mota-Solis N, Wu XH. Pre-yielding and pre-yield cracking in Tial-based alloys. Intermetallics 2006;14(1):82–90. doi:10.1016/j.intermet.2005.04.016.
[46] Couret A, Molénat G, Galy J, Thomas M. Microstructures and mechanical properties of Tial alloys consolidated by spark plasma sintering. Intermetallics 2008;16(9):1134–41. doi:10.1016/j.intermet.2008.06.015.
[47] Kim YW. Strength and ductility in Tial alloys. Intermetallics 1998;6(7):623–8.
[48] Appel F, Oehring M. Gamma-titanium aluminide alloys: alloy design and properties. In: Leyens C, Peters M, editors. Titanium and titanium alloys: fundamentals and applications. Wiley-VCH; 2003. p. 89–152. ISBN 3527305343 [chapter 4].
[49] Kad BK, Asaro RJ. Apparent Hall-Petch effects in polycrystalline lamellar Tial. Philosophical Magazine A 1997;75(1):87–104.